JOURNAL OF PROPULSION AND POWER
Vol. 21, No. 3, May–June 2005

Numerical Modeling of Single-Pulse Gasdynamics and Performance of Pulse Detonation Rocket Engines

C. I. Morris*
NASA Marshall Space Flight Center, Huntsville, Alabama 35812

Pulse detonation rocket engines (PDREs) offer potential performance improvements over conventional designs but represent a challenging modeling task. A quasi-one-dimensional, finite rate chemistry computational fluid dynamics model for PDREs is described and implemented. Four different PDRE geometries are evaluated in this work: a baseline detonation tube, a detonation tube with a straight extension, and a detonation tube with two types of converging/diverging (CD) nozzles. The effect of extension length and CD nozzle area ratio on the single-pulse gasdynamics and performance of a PDRE is studied over a wide range of blowdown pressure ratios (1–1000). The results indicate that a CD nozzle is generally more effective than a straight extension in improving PDRE performance, particularly at higher pressure ratios. Additionally, the results show that the blowdown process of the CD nozzle systems could be beneficially cut off well before the pressure at the endwall reaches the ambient value. The single-pulse performance results are also compared to some recent experimental measurements as well as a steady-state rocket system using similar modeling assumptions.

Nomenclature

A	=	preexponential constant in Arrhenius relation
c_v	=	specific heat at constant volume
D	=	diameter
E	=	activation energy in Arrhenius relation
e	=	specific internal energy
F	=	Troe correction factor for pressure-dependent reactions
F_c	=	Troe centering parameter for pressure-dependent reactions
$\boldsymbol{F}$	=	inviscid convective flux vector
$\boldsymbol{H}$	=	source vector for area change
I_{sp}	=	specific impulse
$\boldsymbol{J}$	=	Jacobian of $\boldsymbol{W}$ with respect to $\boldsymbol{U}$
k_b	=	backward reaction rate
k_{eq}	=	equilibrium constant
k_f	=	forward reaction rate
k_∞	=	high-pressure rate limit of pressure-dependent reactions
k_0	=	low-pressure rate limit of pressure-dependent reactions
L	=	length
M	=	molecular mass
N_r	=	number of reactions
N_s	=	number of species
P_r	=	reduced pressure for pressure-dependent reactions
p	=	gas pressure
$\mathcal{R}$	=	universal gas constant
$S(x)$	=	cross-sectional area as a function of x
T	=	gas temperature
t	=	time from detonation initiation
t_b	=	blowdown time; point in blowdown history when $p_w = p_a$
t_z	=	point in blowdown history when thrust first drops to zero
U	=	wave velocity in the x direction
$\boldsymbol{U}$	=	state vector
u	=	gas velocity in the x direction
V	=	volume
$\boldsymbol{W}$	=	source vector for finite rate chemistry
w	=	source term for finite rate chemistry
x	=	distance from endwall
Y	=	mass fraction
β	=	temperature exponent in Arrhenius relation
γ	=	ratio of specific heats
$\Delta_f h$	=	heat of formation
ε	=	nozzle area expansion ratio, S_x/S^*
ν	=	stoichiometric coefficient in chemical reaction
ρ	=	gas density
υ	=	volume ratio
ψ	=	blowdown pressure ratio, p_i/p_a

Subscripts

a	=	ambient condition
CJ	=	Chapman–Jouguet state
c	=	pertaining to the converging section of a nozzle
d	=	pertaining to the diverging section of a nozzle
e	=	pertaining to a straight tube extension
i	=	initial fill condition in the detonation tube
j	=	reaction index
k, l	=	species indices
m	=	subiteration counter in predictor–corrector integration scheme
t	=	pertaining to the detonation tube
w	=	condition at the endwall of the detonation tube
x	=	pertaining to the exit of a nozzle

Superscripts

n	=	time level index
$\circ$	=	standard state (298.15 K, 1 bar)
$*$	=	throat of a nozzle
$'$	=	reactant side of a chemical reaction
$''$	=	product side of a chemical reaction

Presented as Paper 2004-0463 at the AIAA 42nd Aerospace Sciences Meeting, Reno, NV, 5–8 January 2004; received 26 January 2004; revision received 4 October 2004; accepted for publication 27 September 2004.

*Research Engineer, TD40/Propulsion Research Center. Member AIAA.

Introduction

PULSE detonation engines (PDEs)[1] have generated considerable research interest in recent years as a chemical propulsion system potentially offering improved performance and reduced complexity compared to conventional gas turbines and rocket engines. The detonative mode of combustion employed by these devices offers a theoretical thermodynamic advantage over the constant-pressure

deflagrative combustion mode used in conventional engines. However, the unsteady blowdown process intrinsic to all pulse detonation devices has made realistic estimates of the actual propulsive performance of PDEs problematic. The recent review article by Kailasanath[2] highlights some of the progress that has been made in comparing the available experimental measurements with analytical and numerical models.

The pulse detonation rocket engine (PDRE)[3] has received comparatively more limited research interest than the PDEs intended for airbreathing use. While conceptually similar, the rocket application of this technology requires investigation of the performance characteristics over a wide range of ambient pressures. In conventional rocket engine designs, the converging/diverging (CD) nozzle plays a critical role in converting the thermal energy of the combustion products in the combustion chamber to directed kinetic energy in the exhaust.[4] Thus, there has been considerable recent research interest in studying the use of nozzles for enhancing PDE performance.[5] No attempt is made here to provide an exhaustive review of nozzle research for PDEs, but the most recent results, relevant to the rocket application and the current study, should be listed.

A significant number of studies have examined the effect of straight extensions and nozzles on PDEs filled with propellants at 1 atm and exhausting to air at an ambient pressure of 1 atm. Cooper and Shepherd[6] developed a partial-fill model for modeling the effect of straight extensions and diverging nozzles on detonation tubes at these conditions. This model makes use of the available experimental impulse data in the literature and the partial-fill numerical simulations of Li and Kailasanath.[7] Cambier and Tegner,[8] and more recently Yungster,[9] have also performed single-pulse numerical studies in this regime. They found that single-pulse performance could be significantly improved with diverging nozzles. In contrast, Guzik et al.[10] developed a method of characteristics model for PDEs and found that an idealized, zero-length, dynamically optimized, variable-area nozzle could only modestly (~13%) improve PDE performance at these conditions. Thus, as noted in Ref. 6, in this regime, the volume of the extension or nozzle appears to be the principal driver of performance at these conditions.

An experimental study of the effects of nozzles and extensions on the single-pulse performance of detonation tubes over a wide range of ambient pressures has recently been reported by Cooper and Shepherd.[11] The authors found that the partial-fill tamping effect dominates nozzle/extension performance improvements at low pressure ratios, whereas nozzle flow expansion processes dominate performance gain at high pressure ratios. A limited comparison of these results with the computational fluid dynamics (CFD) model of this work will be discussed in a later section.

Several numerical studies over a variety of fill and ambient pressures have also been reported. Multiple-pulse simulations at elevated injection pressure were performed in Refs. 8 and 9, and both authors found that the nozzle performance improvements could be degraded by nozzle overexpansion losses in the purging and refilling process. Cambier[12] performed a numerical simulation of a PDRE filled initially to 10 atm and fitted with a CD nozzle. He found that the single-pulse performance was consistent with a comparable constant-volume combustor fitted with a similar CD nozzle. Mohanraj and Merkle[13] found in their simulations that both diverging and CD nozzles could improve multiple-pulse PDRE performance at low ambient pressures. A study incorporating multiple tubes into a common nozzle was performed by Mohanraj et al.[14] Although primarily directed toward an airbreathing configuration at altitude of 9.3 km, the studies of Wu et al.[15] and Ma et al.[16] also demonstrate notable (~45%) multiple-pulse PDE performance increases from a CD nozzle. Talley and Coy[17] have developed a zero-dimensional, constant-γ model for studying the performance of an idealized constant-volume combustor with a nozzle over a wide range of pressure ratios.

In a previous paper by the author,[18] parametric studies of the single-pulse performance of a single, straight detonation tube were reported over a wide range of pressure ratios. A one-dimensional, unsteady method of characteristics code, employing a constant-γ assumption behind the detonation front, was developed for that study.

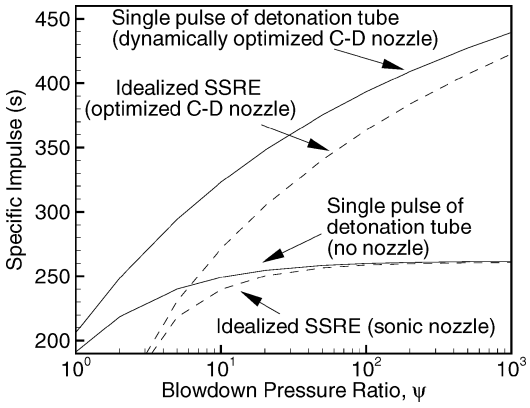

Fig. 1 Constant-γ performance comparison of single-pulse PDREs with conventional SSREs at the same injection pressure (propellant mixture: stoichiometric H_2/O_2 at $p_i = 1$ atm, $T_i = 300$ K).

Models of this type are computationally inexpensive and may be used to illustrate the critical role of nozzles in the rocket PDE application. For example, a plot showing the specific impulse of various PDRE and steady-state rocket engine (SSRE) configurations as a function of blowdown pressure ratio, $\psi = p_i / p_a$, is shown in Fig. 1. The calculations assume a propellant gas mixture of stoichiometric H_2/O_2 at $p_i = 1$ atm, $T_i = 300$ K. In each simulation, execution stops when the pressure at the endwall decays to the ambient value: $p_w = p_a$. Note that the SSRE performance calculations employ the same constant-γ assumption used in the PDRE calculations. There are four performance curves in the figure: an SSRE with a sonic nozzle, an SSRE equipped with an optimized CD nozzle at each pressure ratio, a single pulse from a simple detonation tube, and a single pulse from a detonation tube fitted with an idealized, zero-length dynamically optimized CD nozzle throughout the blowdown process. The clear performance improvement of CD nozzles at high blowdown pressure ratios is evident from the figure. Although a dynamically optimized nozzle is a considerable idealization, these simple constant-γ results clearly demonstrate the critical role that nozzles play in the performance of PDREs, particularly at the high pressure ratios typical for boost or in-space rocket applications.

The purpose of this paper is to study the effect of straight extensions and CD nozzles on the single-pulse gasdynamics and performance of PDREs. Details of the quasi-one-dimensional, finite rate chemistry CFD model developed by the author are provided first. This model, although still highly idealized, permits study of these issues in greater detail than can be obtained using the previous constant-γ method of characteristics approach. Four different PDRE geometries are evaluated: a baseline detonation tube, a detonation tube with a straight extension, and a detonation tube with two types of CD nozzles. The effect of extension length and CD nozzle area ratio on the single-pulse gasdynamics, performance, and blowdown time of a PDRE is studied over a wide range of blowdown pressure ratios (1–1000). The overall effectiveness of straight extensions and CD nozzles in improving performance is evaluated. These single-pulse results are also compared to some recent experimental measurements, as well as a steady-state rocket system using similar modeling assumptions.

Governing Equations

The quasi-one-dimensional Euler equations are the governing model used in this study. A quasi-one-dimensional model is at best an approximation of a PDRE or SSRE. Real detonation waves exhibit clear multidimensional behavior, and multidimensional effects can also in some cases affect the flow near the tube exit. Additionally, flow separation in rocket engine nozzles is strongly dependent on multidimensional and viscous effects. However, because the primary goal of this study is to determine the effect of extensions and nozzles on pulse detonation rocket systems to first order, the quasi-one-dimensional Euler equations were deemed a reasonable model. Moreover, previous studies[12,19,20] have indicated that, for impulse

calculations, the quasi-one-dimensional approach (with zero pressure relaxation length at the exit plane) generally agrees well with single-pulse two-dimensional simulations of simple detonation tubes and nozzles. The time-dependent form of these equations, including the effect of finite rate chemistry, is written as follows:

$$\frac{\partial \boldsymbol{U}}{\partial t} + \frac{1}{S}\frac{\partial \boldsymbol{F}S}{\partial x} = \boldsymbol{H} + \boldsymbol{W} \tag{1}$$

where the state vector $\boldsymbol{U}$ and inviscid convective flux vector $\boldsymbol{F}$ are given by

$$\boldsymbol{U} = \begin{bmatrix} \rho_1 \\ \rho_2 \\ \vdots \\ \rho_{N_s} \\ \rho u \\ \rho\left(e + \frac{1}{2}u^2\right) \end{bmatrix}, \qquad \boldsymbol{F} = \begin{bmatrix} \rho_1 u \\ \rho_2 u \\ \vdots \\ \rho_{N_s} u \\ \rho u^2 + p \\ \rho u\left(e + \frac{1}{2}u^2\right) + pu \end{bmatrix} \tag{2}$$

and the source vectors accounting for the effect of area change, $\boldsymbol{H}$, and for the effect of finite rate chemistry, $\boldsymbol{W}$, are

$$\boldsymbol{H} = \begin{bmatrix} 0 \\ 0 \\ \vdots \\ 0 \\ \dfrac{p}{S}\dfrac{\partial S}{\partial x} \\ 0 \end{bmatrix}, \qquad \boldsymbol{W} = \begin{bmatrix} w_1 \\ w_2 \\ \vdots \\ w_{N_s} \\ 0 \\ 0 \end{bmatrix} \tag{3}$$

The gas density ρ is the sum of the individual species densities,

$$\rho = \sum_{k=1}^{N_s} \rho_k$$

whereas the gas pressure p is given by the ideal gas law;

$$p = \sum_{k=1}^{N_s} (\rho_k / M_k)\mathcal{R}T$$

The specific internal energy e is given by

$$e(T) = \sum_{k=1}^{N_s} Y_k \left[\int_{T^o}^{T} c_{v_k}(T)\,\mathrm{d}T + \Delta_f h_k^\circ \right] \tag{4}$$

and is used for the implicit evaluation of temperature by Newton–Raphson iteration. The mass fraction Y is given by $Y_k = \rho_k/\rho$.

In this work, the ideal gas thermodynamic fits of McBride et al.[21] are used to calculate the internal energy, specific heat, and Gibbs free energy for the $N_s = 9$ species in the problem (N_2, O_2, H_2, OH, H_2O, H, O, HO_2, and H_2O_2).

Chemistry Model

The source terms for finite rate chemistry, w_k in Eq. (3), are calculated from the sum of relevant chemical reactions for each species. Thus, for a chemical mechanism of N_r elementary reactions, each reaction is expressed as

$$\sum_{l=1}^{N_s} \nu'_{l,j} X_l \rightleftharpoons \sum_{l=1}^{N_s} \nu''_{l,j} X_l \tag{5}$$

where $\nu'_{l,j}$ are the stoichiometric coefficients of species l on the reactant side of reaction j, while $\nu''_{l,j}$ are the corresponding stoichiometric coefficients on the product side. The production term for each species k may be written as

$$w_k = M_k \sum_{j=1}^{N_r} \left(\nu''_{k,j} - \nu'_{k,j}\right) \left[k_{f_j} \prod_{l=1}^{N_s} \left(\frac{\rho_l}{M_l}\right)^{\nu'_{l,j}} - k_{b_j} \prod_{l=1}^{N_s} \left(\frac{\rho_l}{M_l}\right)^{\nu''_{l,j}} \right] \tag{6}$$

Details of the chemical kinetics mechanism for H_2/O_2 combustion used in this work are shown in Table 1. This $N_r = 18$ reaction

Table 1 Chemical kinetics mechanism for H_2/O_2 combustion[22]

Number	Reaction[a]		A[b]	β[b]	E[b]
1	$O + H_2 \rightleftharpoons H + OH$		5.00×10^4	2.70	6,290
2[c]	$H + O_2 + M \rightleftharpoons HO_2 + M$		2.80×10^{18}	−0.90	0
3	$H + O_2 + O_2 \rightleftharpoons HO_2 + O_2$		3.00×10^{20}	−1.70	0
4	$H + O_2 + H_2O \rightleftharpoons HO_2 + H_2O$		9.38×10^{18}	−0.80	0
5	$H + O_2 + N_2 \rightleftharpoons HO_2 + N_2$		2.60×10^{19}	−1.20	0
6	$H + O_2 \rightleftharpoons O + OH$		8.30×10^{13}	0.00	14,413
7	$H + HO_2 \rightleftharpoons O_2 + H_2$		2.80×10^{13}	0.00	1,068
8	$H + HO_2 \rightleftharpoons OH + OH$		1.34×10^{14}	0.00	635
9	$H + H_2O_2 \rightleftharpoons HO_2 + H_2$		1.21×10^7	2.00	5,200
10	$OH + H_2 \rightleftharpoons H_2O + H$		2.16×10^8	1.50	5,200
11[d,e]	$OH + OH + M \rightleftharpoons H_2O_2 + M$	k_∞	7.40×10^{13}	−0.40	0
		k_0	2.30×10^{18}	−0.90	−1,700
12	$OH + HO_2 \rightleftharpoons O_2 + H_2O$		2.90×10^{13}	0.00	−500
13[f]	$OH + H_2O_2 \rightleftharpoons HO_2 + H_2O$	k_a	1.75×10^{12}	0.00	320
		k_b	5.80×10^{14}	0.00	9,560
14[g]	$HO_2 + HO_2 \rightleftharpoons O_2 + H_2O_2$	k_c	1.30×10^{11}	0.00	−1,630
		k_d	4.20×10^{14}	0.00	12,000
15[h]	$O + O + M \rightleftharpoons O_2 + M$		1.20×10^{17}	−1.00	0
16[d]	$O + H + M \rightleftharpoons OH + M$		5.00×10^{17}	−1.00	0
17[i]	$H + OH + M \rightleftharpoons H_2O + M$		2.20×10^{22}	−2.00	0
18[j]	$H + H + M \rightleftharpoons H_2 + M$		1.00×10^{18}	−1.00	0

Note: species are N_2, O_2, H_2, H_2O, OH, H, O, HO_2, H_2O_2.
[a]All reactions are reversible.
[b]$k_f = AT^\beta \exp(-E/RT)$; units are in cal, mol, cm^3, and s.
[c]M does not include O_2, H_2O, or N_2; all collision efficiencies = 1.0.
[d]Collision efficiencies for M; $H_2 = 2.0$, $H_2O = 6.0$, all others = 1.0.
[e]Troe parameters: $a = 0.7346$, $T^{***} = 94$, $T^* = 1756$, $T^{**} = 5182$.
[f]Rate coefficient is non-Arrhenius: $k_{13} = k_a + k_b$.
[g]Rate coefficient is non-Arrhenius: $k_{14} = k_c + k_d$.
[h]Collision efficiencies for M; $H_2 = 2.4$, $H_2O = 15.4$, all others = 1.0.
[i]Collision efficiencies for M; $H_2 = 0.73$, $H_2O = 3.65$, all others = 1.0.
[j]Collision efficiencies for M; $H_2 = 1.7$, $H_2O = 7.0$, all others = 1.0.

mechanism was developed by Petersen and Hanson[22] to model H_2/O_2 ignition at the elevated pressures typical of practical high-speed propulsion systems. The rate coefficients for reactions without pressure dependence take on the conventional Arrhenius form:

$$k_{f_j} = A_j T^{\beta_j} \exp(-E_j/\mathcal{R}T) \tag{7}$$

Pressure-dependent reactions are modeled using the approach given by Kee et al.[23]:

$$k_{f_j} = k_\infty [P_r/(1+P_r)]F \tag{8}$$

where the reduced pressure, P_r, is

$$P_r = k_0[M]/k_\infty \tag{9}$$

and $[M]$ is the mixture concentration (including third-body collision efficiencies); k_0 and k_∞ are calculated using the preceding Arrhenius form. The correction factor F is in the Troe[24] form:

$$\ell n\, F = \left[1 + \frac{\ell n\, P_r + c}{n - d(\ell n\, P_r + c)}\right]^{-1} \ell n\, F_c \tag{10}$$

where the constants $c = -0.4 - 0.67\,\ell n\, F_c$, $n = -0.75 - 1.27\,\ell n\, F_c$, and $d = 0.14$. The Troe centering parameter F_c is given by

$$F_c = (1-a)\exp(-T/T^{***}) + a\exp(-T/T^{*}) + \exp(-T^{**}/T) \tag{11}$$

where a, T^{***}, T^{*}, and T^{**} are Troe constants listed in the mechanism.

All reactions in the mechanism are reversible. The reverse reaction rate for each reaction, k_b, is calculated from the forward rate and the equilibrium constant:

$$k_{b_j} = k_{f_j} \big/ k_{\mathrm{eq}_j} \tag{12}$$

where the equilibrium constant, k_{eq_j}, is calculated using the standard Gibbs free energy difference for each reaction.

Numerical Method

The governing quasi-one-dimensional Euler equations are solved in finite volume form throughout the entire domain. The equations are solved in split form, in which a fluid convection subroutine solves Eq. (1) without the chemistry source vector $\boldsymbol{W}$,

$$\frac{\partial \boldsymbol{U}}{\partial t} + \frac{1}{S}\frac{\partial \boldsymbol{F}S}{\partial x} = \boldsymbol{H} \tag{13}$$

and a finite rate chemistry integration subroutine solves Eq. (1) as a system of ordinary differential equations ignoring $\boldsymbol{F}$ and $\boldsymbol{H}$:

$$\frac{\partial \boldsymbol{U}}{\partial t} = \boldsymbol{W} \tag{14}$$

The code utilizes the Strang[25] second-order time step splitting approach to couple the fluid convection and finite rate chemistry subroutines. For each complete time step, the chemistry subroutine is first called for one-half of a time step, followed by a full fluid convection time step, and then followed by another half-step of the chemistry routine. The time-step splitting approach allows both high-quality fluid and chemical solvers to be developed and tested independently and then joined together in relatively straightforward fashion. As described by Oran and Boris,[26] time-step splitting generally works well when relatively small time steps are used. However, in the presence of stiff source terms, special care must be taken with this method. This point is developed further later in the paper.

The fluid solver used here is the explicit, second-order-accurate (in time and space), symmetric total variation diminishing algorithm described by Yee.[27] The solver employs Roe's approximate Riemann solver modified for nonequilibrium ideal gases.[28] It also incorporates suggestions by Larrouturou[29] to ensure species positivity.

As with most reactive flow problems, the time integration of the chemistry mechanism in this work requires a stiff ordinary differential equation (ODE) solver to ensure accuracy. The method used here employs a semi-implicit trapezoidal scheme as a predictor:

$$\left[\boldsymbol{I} - \tfrac{1}{2}\Delta t \boldsymbol{J}\right]\left(\boldsymbol{U}_{(1)}^{n+1} - \boldsymbol{U}^n\right) = \Delta t \boldsymbol{W}^n \tag{15}$$

where $\boldsymbol{I}$ is the identity matrix, and $\boldsymbol{J}$ is the Jacobian of $\boldsymbol{W}$ ($\boldsymbol{J} = \partial \boldsymbol{W}/\partial \boldsymbol{U}$). Newton iteration of the trapezoidal scheme is used as a corrector:

$$\left[\boldsymbol{I} - \tfrac{1}{2}\Delta t \boldsymbol{J}\right]\left(\boldsymbol{U}_{(m)}^{n+1} - \boldsymbol{U}_{(m-1)}^{n+1}\right) = \boldsymbol{U}^n - \boldsymbol{U}_{(m-1)}^{n+1} + \tfrac{1}{2}\Delta t\left(\boldsymbol{W}^n + \boldsymbol{W}_{(m-1)}^{n+1}\right) \tag{16}$$

The chemistry integration subroutine is designed to use several substeps, if necessary for accuracy, within a given global half-step. The substeps are chosen such that no species concentration is predicted to change by more than 1% within each substep. Naturally, this leads to more extensive use of substeps when the species concentrations within a computational cell are far from equilibrium. The Jacobian $\boldsymbol{J}$ is evaluated analytically once per substep at $\boldsymbol{U}^n$. Thus, the lower-upper factorization (LU) decomposition of the bracketed matrix terms on the left-hand side of Eq. (15) can be reused in Eq. (16). Two corrector iterations were performed per substep ($m = 2-3$).

As shown by Colella et al.[30] and Leveque and Yee,[31] the presence of stiff source terms in the governing equations can result in nonphysical wave speeds if the grid spacing is too coarse. Additionally, the latter authors point out that improvements to the ODE solver, which potentially reduce spurious overshoots in the solution, cannot solve this problem. Because this issue is fundamentally related to grid resolution, an analysis of the effect of grid resolution on computed detonation wave speed is provided in the next section.

PDRE Simulations

The four different PDRE geometries studied in this work (Fig. 2) are highly idealized. Each is based on a constant-area ($D_t = 2.0$ cm) detonation tube ($L_t = 20$ cm). One end of the detonation tube is closed, while the other is either open to the environment (geometry A), attached to a straight extension (geometry B), or a CD nozzle section (geometries C and D). Geometry A represents the baseline case. Four different straight extensions for geometry B were evaluated in this study: $L_e = 4.0$, 10, 20, and 40 cm. These extensions correspond to ratios of the total assembled tube volume to the detonation tube volume of $\upsilon = 1.2$, 1.5, 2.0, and 3.0. In both of the CD nozzle geometries (C and D), the half-angle in the converging section is 15 deg. The primary difference between the two geometries is that in C the length of the converging section is $L_c = 0.4$ cm, whereas in D this length is $L_c = 1.2$ cm. This results in a nozzle throat diameter for geometry C of $D^* = 1.786$ cm and for geometry

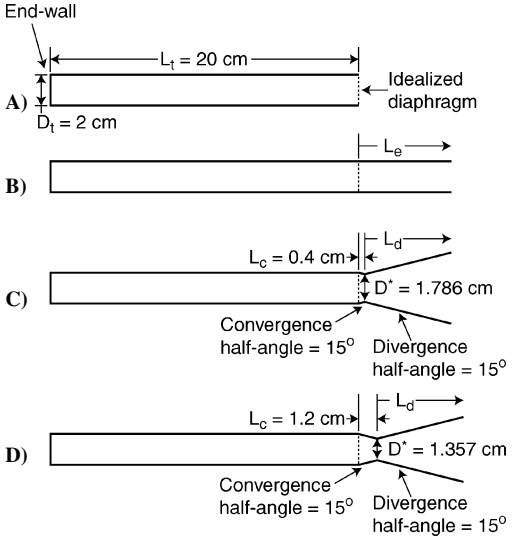

Fig. 2 Schematic of PDRE geometries studied.

D of $D^* = 1.357$ cm. Thus, the maximum rate of outflow is more restricted in geometry D than in C and in both cases is less than that of baseline geometry A. The half-angle in the diverging section of the nozzle is fixed at 15 deg in both geometries. The length of the diverging section, L_d, is a variable set at run time, which is detailed in the results and discussion to follow. The CD nozzle area ratio, ε, is defined throughout this work as the ratio of the nozzle area at the exit plane to the throat area.

The detonation tube is prefilled with a gaseous propellant mixture with no initial velocity. Stoichiometric H_2/O_2 at $p_i = 1$ atm, $T_i = 300$ K is utilized for all calculations in this work. An idealized, massless diaphragm isolates the propellant mixture from the nozzle and ambient environment until ruptured by the detonation wave. The extension or nozzle section is initially filled with H_2 gas at a temperature of 300 K and at the specified ambient pressure. The choice of the ambient gas has a nontrivial impact on the impulse of geometries B, C, and D in single-pulse simulations. Moreover, a number of options can be reasonably selected. Hydrogen is used here primarily due to its low molecular weight, which allowed a wide range of ambient conditions to be studied using the thermochemical model explained previously. The impact of using other possible choices will be addressed in a limited form in the Results and Discussion section.

Detonation initiation is facilitated by calculating the equilibrium combustion conditions (computed at constant density and internal energy) for stoichiometric H_2/O_2 at 10 atm and 3000 K and then specifying these conditions in the computational cell adjacent to the closed endwall. This initiation strategy results in complete formation of the characteristic Chapman–Jouguet (CJ) detonation, Taylor expansion wave, and "plateau" region by $t = 2\,\mu$s. At this point in time the detonation wave is approximately 5 mm from the endwall, or 2.5% of the detonation tube length. It should be noted that this initiation method is specific to the propellant gas mixture and grid resolution used in this study. Less sensitive mixtures, or higher grid resolutions, will typically require a higher "driver" pressure and/or additional cells.

Ghost cells are utilized to specify the boundary conditions in the problem. A reflection-type boundary condition is utilized at the closed end of the detonation tube to simulate a solid wall. The method of characteristics approach of Poinsott and Lele[32] is used to calculate the exit flow boundary condition. For sonic (choked) or supersonic exit flow, all exit flow properties are determined by the interior flow. For subsonic exit flow, the ambient pressure is specified and the method of characteristics is used to compute the remaining flow properties. If reverse flow is detected at the exit, a subsonic inflow boundary condition is calculated using the ambient H_2 gas as a constant-pressure and -enthalpy reservoir.

Two additional special restrictions are imposed in the simulations. To simulate the effect of an idealized diaphragm, only the detonation-tube portion of the domain (from the closed wall to the diaphragm location) is computed initially. A reflection-type boundary condition is specified at the diaphragm location until the pressure in the adjacent cell rises 1.0% above the initial fill value. This special restriction is subsequently removed, and the entire domain is computed. Additionally, there is a check performed when the exit flow is supersonic. Because in this case the exit boundary conditions are entirely calculated from the interior flow, there is no way for the exit flow to return to a subsonic condition.[13] Therefore, at each time step a check is made to determine if the pressure from a standing normal shock at the exit is less than the ambient pressure. If true, then the normal shock properties are specified in the last interior cell, and a subsonic outflow boundary condition is computed at the exit.

Grid Resolution

Grid resolution is a critical issue in all finite rate chemistry CFD models. Due to the extremely fast kinetics of the H_2/O_2 system, numerical modeling of the reaction zone of undiluted H_2–O_2 CJ detonations requires an exceptionally fine grid spacing. The CJ detonation velocity of stoichiometric H_2/O_2 at $p_i = 1$ atm, $T_i = 300$ K is calculated by the NASA CEA thermochemical code[33] to be 2837.1 m/s. Using this velocity, the aforementioned chemical kinetic mechanism, and the ZND computer program of Shepherd,[34] the length of the induction zone behind a steady CJ wave can be calculated as 0.03 mm. Similarly, the length at which the Mach number, in the wave reference frame, behind a steady CJ wave would be 0.75 is 0.11 mm, whereas the point at which the Mach number would be 0.90 is 0.34 mm. A number of other authors[35–37] have recently studied one-dimensional detonation instability using detailed finite rate chemistry. These authors used grid spacings ranging from 80 to ~200 points per steady CJ induction zone length. A comparable resolution for this system would result in a grid spacing of 0.1–0.3 μm. Additionally, the recent work of Powers and Paolucci[38] has shown that a grid spacing roughly three orders of magnitude smaller than the steady CJ induction zone length is necessary to accurately resolve the steady reaction zone structure of all species for a stoichiometric H_2/air detonation. Although not identical to this system, a similar ratio applied here would result in grid spacing less than 0.1 μm. This is not currently practical, nor is it necessary for the performance estimates of this study. The chief requirement here is that the grid resolution accurately calculate the CJ state and velocity.

To assess the effect of grid resolution on the CJ state and wave velocity, the solution was computed for a range of grid spacings from $\Delta x = 0.04$ to 4 mm. For each resolution, the solutions at $t = 30$ and 50 μs after initiation were compared to determine the wave velocity. A grid spacing of $\Delta x = 1$ mm produces an approximately correct CJ detonation wave velocity of ~2900 m/s, whereas a spacing of $\Delta x = 4$ mm yields a clearly nonphysical wave velocity of ~4200 m/s.

A comparison of pressure and temperature profiles of a propagating CJ detonation (at $t = 30\,\mu$s) for the four finest grid spacings is shown in Fig. 3. The resolutions shown in the figure vary over one order of magnitude. Because even the finest resolution shown here, $\Delta x = 0.04$ mm, is larger than the estimated induction zone size, none of the resolutions can accurately capture the ignition process behind the leading shock wave. Rather, in all cases, the propagating CJ detonation is smeared over several cells, resulting in the pressure spike and subsequent relaxation toward the CJ state in the

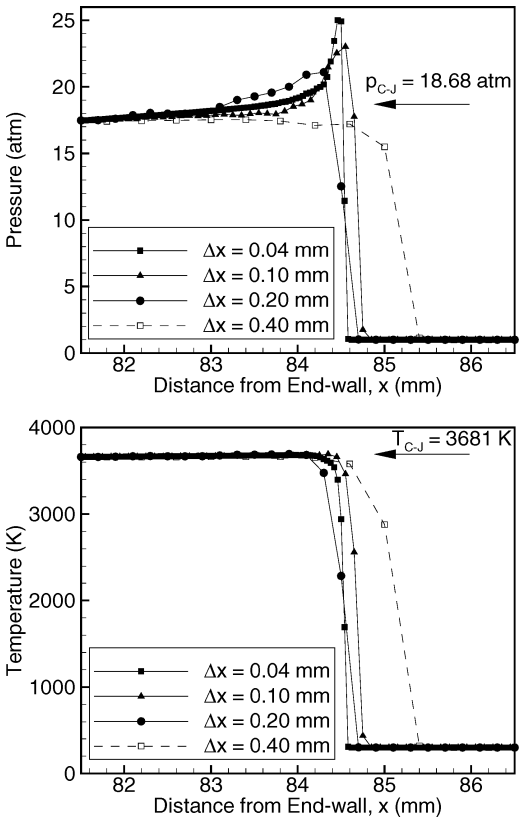

Fig. 3 Grid resolution comparison showing pressure (upper panel) and temperature (lower panel) profiles of a propagating CJ detonation wave at $t = 30\,\mu$s after initiation.

finer grids. All four resolutions capture the detonation velocity with reasonable accuracy (~2836 m/s for $\Delta x = 0.04$ mm, ~2840 m/s for the other resolutions), though the precision of this estimate is naturally lower for the coarser grids. Note, however, that in the two finer grids the pressure relaxes to the CJ value in a significantly shorter distance than in the coarser grids. Based on these observations, a uniform grid spacing of $\Delta x = 0.10$ mm was utilized for all simulations in this study. A Courant–Friedrichs–Lewy number of 0.9 was utilized for all simulations, resulting in a typical time step of $\Delta t \sim 2 \times 10^{-8}$ s.

Thrust Calculations

The time-dependent thrust is calculated at each time step by two different methods. One measure of the thrust assumes a control volume tightly bounding the solid surfaces of the PDRE and is determined by integrating the pressure difference across all surfaces. A second measure assumes a rectangular control volume encapsulating the PDRE. This measure of thrust is determined from the sum of the time rate of change of the internal momentum integral across the domain, the momentum flux from the nozzle section, and the pressure difference across the control volume. In general, there is excellent agreement between the two thrust calculations, and the time-integrated impulse calculations agree to within 0.1%. In all simulations, the calculation proceeds until the pressure at the closed endwall decreases to the ambient value ($p_w = p_a$). The author wishes to emphasize that these simulations should be thought of as single-pulse results.

Results and Discussion

There are several critical factors that can impact the single-pulse performance of a PDRE system. The blowdown pressure ratio is one of the most important parameters governing the performance of any rocket-type system. Additionally, the length of a straight extension, or the area ratio of a CD nozzle, can have a large effect on PDRE performance. In the following section, the essential gasdynamics of the blowdown process in the four PDRE geometries is reviewed. This is followed by a parametric study of the effect of blowdown pressure ratio, extension length, and CD nozzle area ratio on specific impulse and blowdown time. The relative effectiveness of straight extensions and CD nozzles in improving performance is compared. A limited study of the effect of the ambient gas selection on the results is also provided. Additionally, the model predictions are compared with some recent experimental measurements. A comparison of the single-pulse performance of a PDRE fitted with an optimized CD nozzle with an equivalent steady-state rocket engine is also given.

PDRE Blowdown Gasdynamics

The single-pulse blowdown gasdynamics of a detonation tube is generally well known. The recent article by Wintenberger et al.[39] reviewed much of the analytical work to date and proposed a simple analytical model for the blowdown process and impulse. The discussion here briefly reviews the essential wave mechanics and blowdown process in a detonation tube as well as illustrates the effect of a straight extension or CD nozzle on the flowfield. It should be emphasized that the example cases discussed next are chosen primarily for illustrative value.

The blowdown process of a PDRE can be thought of as occurring in several different phases, typically differentiated by the location of important wave structures in the tube. Consider the simplest geometry, the baseline detonation tube (geometry A), using the standard initial conditions and $p_a = 0.01$ atm ($\psi = 100$). A space-time diagram showing Mach-number contours (in increments of 0.1) is shown for this case in the upper panel of Fig. 4. The distance along the tube has been normalized by L_t, while the time has been normalized by $L_t/U_{\mathrm{CJ}} = 70.495$ μs, which is the characteristic time for a CJ detonation to traverse the detonation tube. Additionally, pressure profiles in the detonation tube, at normalized times of $tU_{\mathrm{CJ}}/L_t = 0.5$, 2.5 and 6.0, are shown to the right of the space-time diagram. The detonation is initiated at the endwall at $t = 0$. The subsequent propagation of the detonation wave is clearly shown in the pressure profile for $tU_{\mathrm{CJ}}/L_t = 0.5$. The sharp pressure rise associated with the detonation front is followed by a Taylor expansion wave, which acts to slow and expand the combustion products behind the detonation front. Well behind the detonation front, the products reach a steady pressure at zero forward velocity. Once the detonation reaches the exit of the tube and breaks the idealized diaphragm, outflow begins, and a left-running expansion wave propagates back upstream. This expansion wave expands and accelerates the combustion products toward the exit and is visible in the $tU_{\mathrm{CJ}}/L_t = 2.5$ profile. Once this expansion reaches the endwall, it reflects and begins propagating back downstream toward the exit again. Eventually, the expansion wave reaches the tube exit and further reduces the pressure at that location ($tU_{\mathrm{CJ}}/L_t = 6.0$). Note at the longer times that the Mach-number distribution increases in a relatively uniform fashion from zero at the endwall to unity at the tube exit. The endwall pressure, p_w, for this case is shown in a solid line as a function of normalized time in Fig. 5. Note that p_w is steady at a "plateau" value until the primary expansion wave reaches the endwall.

The addition of an extension to the detonation tube (geometry B) primarily serves to increase the amount of time required for some of the waves to traverse the tube. A space-time diagram, and representative pressure profiles, of a detonation tube with $L_e = 10$ cm extension section are shown in the lower panel of Fig. 4. As before, $\psi = 100$. As in the baseline case, a left-running expansion wave is initiated when the detonation reaches the end of the detonation tube. Additionally, because there is no combustible gas mixture in the extension, the detonation wave changes into a transmitted shock wave in the extension. As may be seen from the space-time diagram, when the transmitted shock reaches the exit of the extension section, it is followed by a period of unsteady supersonic outflow from the tube. Eventually, however, a quasi-steady subsonic flow is established throughout the entire tube. This leads to pressure profiles quite similar to the baseline case. Note from examining Fig. 5 that the overall effect of the extension is to slow the rate of pressure relaxation at the endwall.

A CD nozzle has a significant effect on the flowfield of a PDRE. Space-time diagrams and representative pressure profiles are shown for two CD nozzle example cases in the upper panel (geometry C with $L_d = 9.6$ cm) and lower panel (geometry D with $L_d = 8.8$ cm) of Fig. 6. In both cases ψ is again 100. As was the case previously, a left-running expansion wave, initiated when the detonation reaches the end of the detonation tube, is a key factor in controlling the pressure relaxation at the endwall. However, it is clear from examining the figures that the CD nozzle acts to expand the combustion products to a much lower exit pressure than would otherwise be accomplished by the detonation tube alone. The primary difference between the two CD nozzle cases is the significantly smaller throat in geometry D, which results in reduced mass outflow compared to geometry C. This flow restriction is significant enough that the left-running expansion wave is led by a weak shock wave, clearly visible in the space-time diagram and $tU_{\mathrm{CJ}}/L_t = 2.5$ pressure profile in the lower panel of the figure. These shock reflections are also clearly visible in the endwall pressure history for geometry D (Fig. 5). Note also in that figure the significantly reduced overall rate of pressure decay at the endwall for geometry D when compared to the other example cases.

The impulse history of all four of these example cases is shown in Fig. 7. The instantaneous thrust can be thought of as the slope of these impulse curves. Note that all four curves are coincident before the detonation wave reaches the idealized diaphragm. As discussed previously, the primary effect of the extension in geometry B is to reduce the rate of pressure relaxation at the endwall. This results in a modestly higher thrust in the later portions of the blowdown history, compared to the baseline geometry A. In contrast, the CD nozzle has a more significant effect on the thrust and impulse. Geometry C initially exhibits a very brief (~3 μs) decrease in instantaneous thrust after the detonation wave breaks the diaphragm and begins to interact with the nozzle. Subsequently, however, geometry C yields a higher thrust and resultant impulse than geometries A or B throughout the remaining portion of the blowdown history. Due to the more restricted mass outflow, and internal shock wave reflections, the

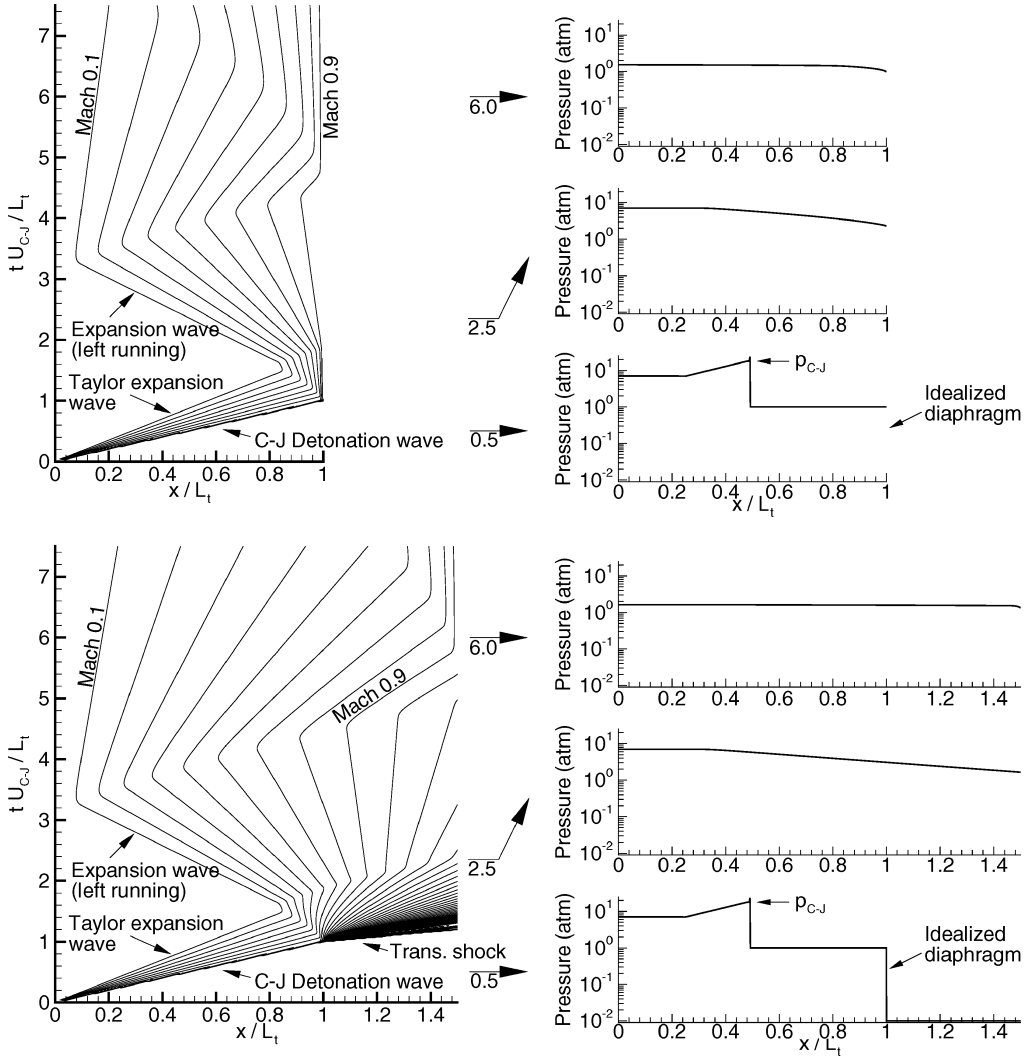

Fig. 4 Space-time diagram showing Mach-number contours and pressure profiles for (upper panel) PDRE geometries A and (lower panel) B with $L_e = 10$ cm extension (propellant mixture: stoichiometric H_2/O_2 at $p_i = 1$ atm, $T_i = 300$ K, $p_a = 0.01$ atm, $\psi = 100$).

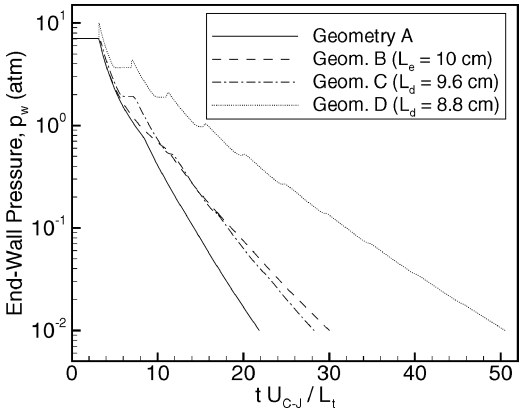

Fig. 5 Pressure history at the endwall for example PDRE geometries; time is normalized by L_t/U_{CJ} (propellant mixture: stoichiometric H_2/O_2 at $p_i = 1$ atm, $T_i = 300$ K, $p_a = 0.01$ atm, $\psi = 100$).

instantaneous thrust in geometry D is generally lower than that of geometry C. However, although the overall blowdown time is significantly longer than for geometry C, the final impulse is nearly equivalent. One additional important observation that can be made from Fig. 7 is that typically the integrated impulse will achieve a value quite close to, or even slightly exceeding, the final value well before the end of the simulation. This is particularly true of the two CD nozzle geometries and is observed over the entire blowdown pressure range studied in this work. This point will be addressed in greater detail in the following sections.

PDRE Performance Results

The performance trends just discussed can be seen in greater detail by studying the single-pulse performance of the various PDRE geometries over a wide range of blowdown pressure ratios. The specific impulse of the baseline detonation tube (geometry A) and the detonation tube with several extension lengths (geometry B with $L_e = 4$, 10, 20, and 40 cm) is shown in Fig. 8. As is evident from the figure, the general performance trends of all five configurations are quite similar. There is a fairly significant improvement in performance (30–38%) over $\psi = 1$–10, but decidedly less so (4–8%) over $\psi = 10$–100. There is very little improvement in performance ($\sim$1%) over $\psi = 100$–1000. In general, there is a definite performance improvement provided by the extension section, and this benefit increases with extension length. The one exception to this trend occurs at $\psi = 2$. In this particular case, there is no additional performance benefit for $L_e > 10$ cm. This is due to the fact that the primary expansion wave, generated at the interface between the detonation tube and the extension section, is alone sufficient to reduce the pressure at the endwall to the ambient value. In this particular case, this event occurs before the secondary expansion wave (generated when the transmitted shock reaches the exit of the extension) can reach the endwall. Thus, there is no effect from the longer extensions at this pressure ratio. At higher blowdown pressure ratios ($\psi = 5$–1000) this phenomena does not occur; the pressure decay (to

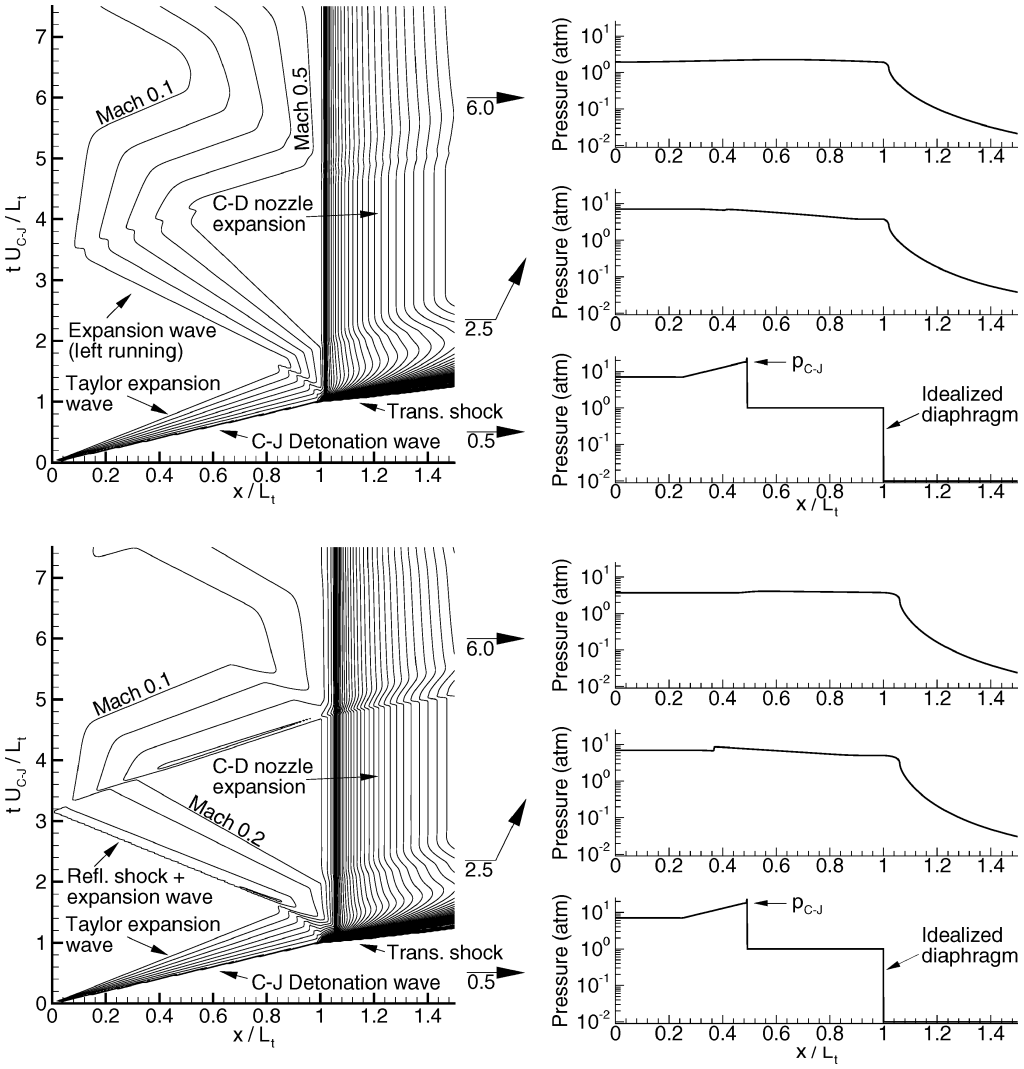

Fig. 6 Space-time diagram showing Mach-number contours and pressure profiles for (upper panel) PDRE geometries C with $L_d = 9.6$ cm and (lower panel) D with $L_d = 8.8$ cm (propellant mixture: stoichiometric H_2/O_2 at $p_i = 1$ atm, $T_i = 300$ K, $p_a = 0.01$ atm, $\psi = 100$).

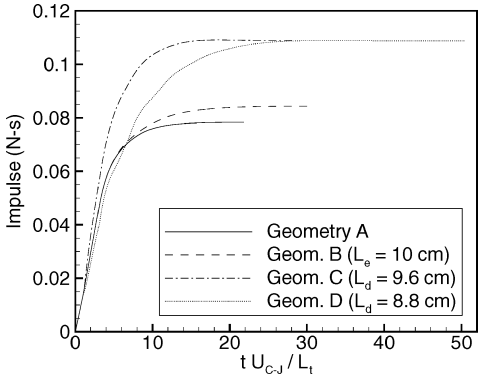

Fig. 7 Impulse history for example PDRE geometries; time is normalized by L_t/U_{CJ} (propellant mixture: stoichiometric H_2/O_2 at $p_i = 1$ atm, $T_i = 300$ K, $p_a = 0.01$ atm, $\psi = 100$).

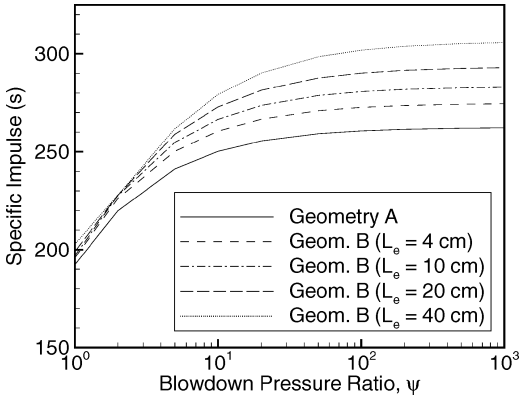

Fig. 8 Effect of blowdown pressure ratio on specific impulse for PDRE geometries A and B. Propellant mixture: stoichiometric H_2-O_2 at $p_i = 1$ atm, $T_i = 300$ K.

ambient) provided by the primary expansion at the endwall is long enough that the secondary expansion wave can reach the endwall in time to affect the pressure relaxation rate.

Both the blowdown pressure ratio ψ and the nozzle area expansion ratio ε play critical roles in the performance of the CD nozzle PDRE geometries. Performance results as a function of CD nozzle area expansion ratio for geometries C and D (upper and lower panels, respectively) are shown in Fig. 9. In each case, ε was adjusted by varying the length of the diverging section of the nozzle (L_d). Results for $\psi = 1$–1000 are plotted. As is the case for conventional rocket-type systems, for a given pressure ratio, the performance gain provided by a CD nozzle will generally increase with ε up to a certain optimum point. After this point performance will decrease with increasing ε. The dashed curve in each graph shows the fixed ε that yields optimum specific impulse for each ψ. It is important to recognize that this optimum point is specific to the propellant, ambient gas, CD nozzle geometry, and blowdown time assumption used.

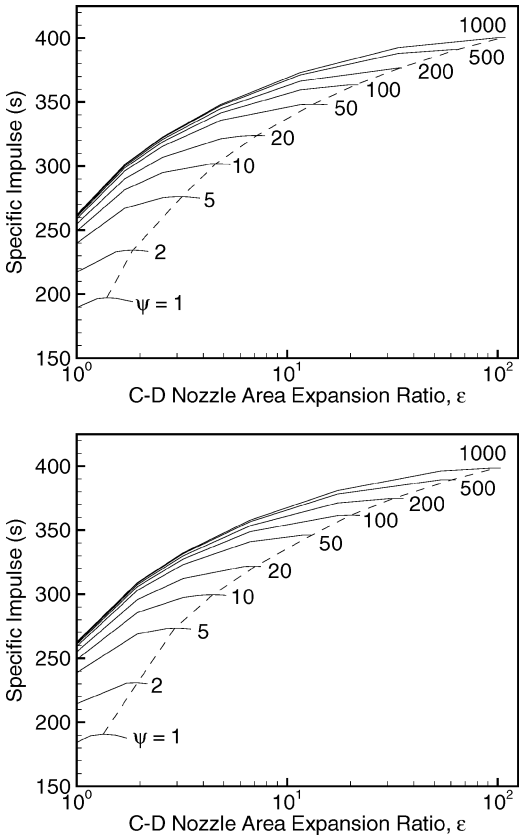

Fig. 9 Effect of expansion ratio on specific impulse for (upper panel) PDRE geometries C and (lower panel) D; dashed line represents the fixed ε giving optimum performance at each ψ (propellant mixture: stoichiometric H_2/O_2 at $p_i = 1$ atm, $T_i = 300$ K).

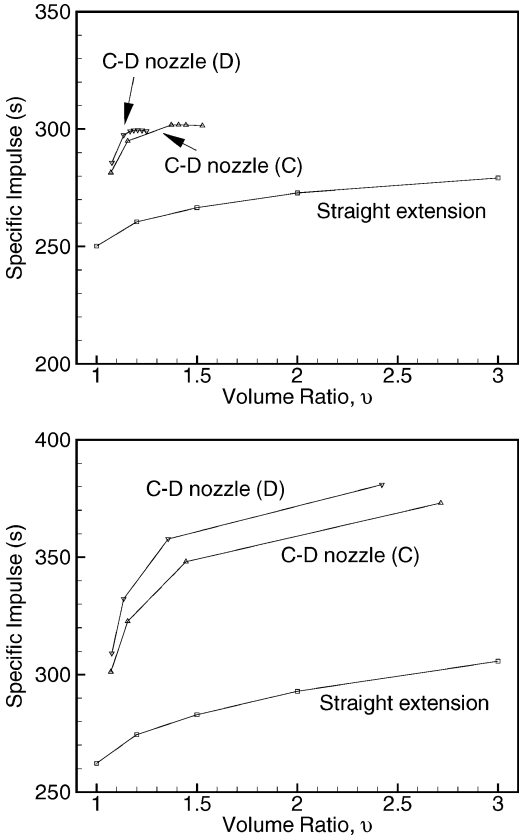

Fig. 10 Specific impulse plotted as a function of volume ratio (upper panel, $\psi = 10$; lower panel, $\psi = 1000$; (propellant mixture: stoichiometric H_2/O_2 at $p_i = 1$ atm, $T_i = 300$ K).

In general, there is little performance difference between the two CD nozzle geometries. The performance of geometry D, for fixed ψ and ε, tends to be slightly lower than that for geometry C, primarily due to losses induced by the reflected shock waves present in the blowdown history of D. Note that a CD nozzle is generally more effective at improving performance at higher pressure ratios than the extensions in geometry B. The specific impulse when using an optimized CD nozzle improves by 53–57% over $\psi = 1$–10 and 20–21% over $\psi = 10$–100. Even over $\psi = 100$–1000, the performance increases by 10%. This is largely due to the ability of a CD nozzle to convert the thermal energy of the combustion products into directed kinetic energy. This effect can also be seen by plotting the specific impulse for all four geometries as a function of volume ratio (Fig. 10). The volume ratio υ is defined here as the ratio of the entire assembled tube volume ($V_t + V_e$, or $V_t + V_c + V_d$) to the detonation tube volume alone, V_t; ψ is 10 in the upper panel of the figure and 1000 in the lower panel. It is evident from the figure that a CD nozzle is generally a more effective use of volume than a straight extension, particularly at relatively high ψ. It should be emphasized, however, that this observation is based on the assumption that the volume ratio range under consideration is within the range where increased nozzle expansion provides improved performance.

PDRE Blowdown Time Results

Because the cycle time of an operational PDRE system is of great practical interest, it is useful to examine the effect of the blowdown pressure ratio, straight extension length, and CD nozzle area expansion ratio on the single-pulse blowdown time of the PDRE geometries considered here. The blowdown time in this work, t_b, is defined as the time at which the pressure at the endwall decays to the ambient value ($p_w = p_a$). The strong dependence of t_b on ψ and extension length can be seen in Fig. 11. Note that, at the highest blowdown pressure ratios, there is an almost directly proportional dependence of blowdown time to extension length. The obvious

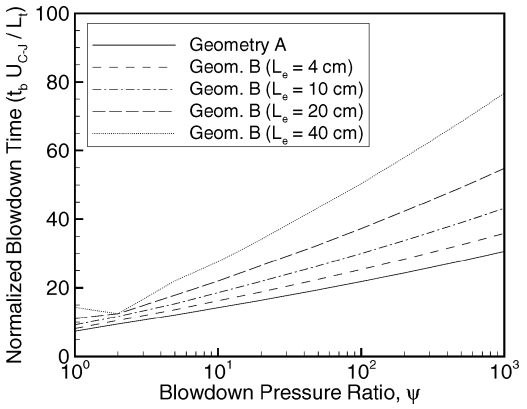

Fig. 11 Normalized blowdown time ($t_b U_{CJ}/L_t$) plotted as a function of blowdown pressure ratio for PDRE geometries A and B (propellant mixture: stoichiometric H_2/O_2 at $p_i = 1$ atm, $T_i = 300$ K).

kink in the $L_e = 20$ and 40 cm curves at $\psi = 2$ was explained in the preceding section.

The blowdown time for the two CD nozzle PDRE geometries is shown in Fig. 12. As would be expected, t_b is consistently longer for geometry D than for C over the entire range of blowdown pressure ratios. Note that these results assume the use of the optimum fixed CD nozzle for each pressure ratio, though because the nozzle throat outflow is nearly always choked, t_b is nearly independent of ε at a given ψ. One of the notable results of these simulations is that the instantaneous thrust of even an optimum fixed CD nozzle is slightly negative for much of the latter portions of the blowdown time. This result is due to the fact that the CD nozzle overexpands the residual combustion products when the pressure in the detonation tube has decayed sufficiently. Thus, it is useful to also plot the time at which the thrust first drops to zero in the blowdown history (t_z). It is evident

Table 2 Effect of ambient gas selection on model results for geometry B[a]

		% Increase I_{sp}			% Increase t_b		
ψ	υ	H_2	He	N_2	H_2	He	N_2
1	1.2	1.84	4.22	22.2	10.6	12.8	21.0
	1.5	2.41	9.16	44.7	25.6	31.2	50.9
	2.0	3.49	15.7	77.3	50.4	59.5	103.0
	3.0	5.49	26.3	134.0	95.0	115.0	228.0
10	1.2	4.13	4.13	4.38	14.1	14.1	14.4
	1.5	6.53	6.53	8.59	30.6	30.6	34.5
	2.0	9.05	9.06	14.9	54.3	54.3	67.0
	3.0	11.6	11.6	25.4	93.7	93.7	128.0
50	1.2	4.52	4.52	4.53	15.6	15.6	15.6
	1.5	7.52	7.52	7.53	35.8	35.8	35.8
	2.0	11.0	11.0	11.1	67.0	67.0	67.0
	3.0	15.1	15.1	15.2	123.0	123.0	123.0

[a]Increases listed are with respect to the value for geometry A at the given ψ.

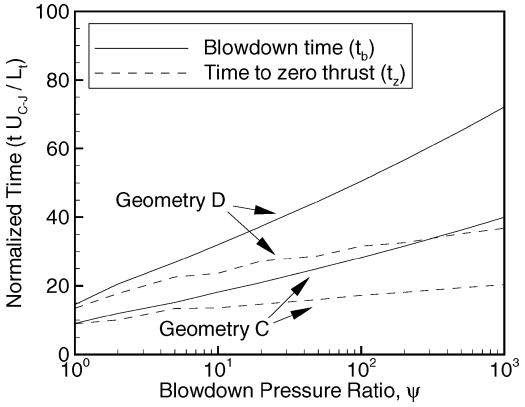

Fig. 12 Normalized time (tU_{CJ}/L_t) plotted as a function of blowdown pressure ratio for PDRE geometries C and D (propellant mixture: stoichiometric H_2/O_2 at $p_i = 1$ atm, $T_i = 300$ K).

from the figure that this point occurs considerably earlier than t_b, particularly at the highest ψ. Because the instantaneous thrust, even while negative, is so small at this point, there is little difference in integrated impulse between these two time points (typically at most a loss of ~1 s of specific impulse over the interval). However, this observation suggests that a considerable savings in overall cycle time could be realized with an actual slight gain in performance. Note that, because the endwall is the only thrust surface for geometries A and B, $t_z = t_b$ for those cases.

Effect of Ambient Gas on Model Results

Because these are single-pulse simulations, it is logical to expect that the choice of the ambient gas in the extension and nozzle sections may influence the performance and blowdown time results. In an operational multicycle PDRE, the gas in these sections would likely be a mixture of the ambient atmosphere, the combustion products from the previous cycle, and any purge gases used in the cycle. Hydrogen is used as the ambient gas in all simulations in this work. However, to form a limited appreciation for the impact of this choice on the results, additional simulations using helium (He) and N_2 as the ambient gas are also conducted at $p_a = 1.0$, 0.1, and 0.02 atm ($\psi = 1$, 10, and 50, respectively) conditions. The ambient temperature remains at 300 K. In effect, due to their higher density, He and particularly N_2 provide a larger tamping mass (2×, and 14×, respectively) at a given pressure, and for a given extension or nozzle volume, than H_2 does (see Ref. 6 for a discussion of this point). The results for straight extensions (geometry B), with respect to the baseline detonation tube (geometry A), are summarized in Table 2.

The most significant effect from ambient gas selection is exhibited at $\psi = 1$. In this case both He and N_2 show large departures in both specific impulse and blowdown time from the H_2 results. The effects are particularly large for N_2 because the density of N_2 is 2.33 times larger than the density of the stoichiometric H_2/O_2 propellant. The greatly reduced sound speed of He and N_2, compared to H_2, results in a much stronger transmitted shock in the extension or CD nozzle sections. In the case of a straight extension, the stronger transmitted shock significantly reduces the pressure variation across the primary left-running expansion wave. This causes a comparatively higher pressure at the endwall before the arrival of the secondary expansion wave (from the exit). Thus, both impulse and blowdown time are increased, though typically blowdown time increases faster than impulse. In the case of a CD nozzle, the resultant high pressure behind this shock causes additional impulse to be transmitted to the diverging section of a CD nozzle. This yields a modest amount (~7 s) of additional impulse for an $\varepsilon = 1.4$ nozzle using N_2 at this condition. Blowdown time is not notably affected. It is fair to point out that the optimum fixed ε for a CD nozzle geometry is typically increased by the use of He and N_2, though an extensive reoptimization is not conducted here.

The ambient gas selection has a much smaller effect on impulse and blowdown time for geometry B at $\psi = 10$ and 50. Although the use of N_2 can provide somewhat modest relative increases in these values at $\psi = 10$, there is essentially no effect from ambient gas selection at $\psi = 50$. The CD nozzle geometries also exhibit small performance gains at these conditions: ~3–5 s for $\varepsilon = 4.4$ at $\psi = 10$, and ~2 s for $\varepsilon = 12.4$ at $\psi = 50$. Again blowdown time is not affected.

In summary, the use of H_2 as the ambient nozzle/extension gas in this work has effectively minimized tamping effects as much as possible in the model. Although this has little effect at high pressure ratios, the sensitivity of the results to this choice near $\psi = 1$ is significant.

Comparison of Model Results with Experiments

Due to the highly idealized nature of these simulations, it is reasonable to expect that the performance predictions will tend to overpredict the experimental results available in the literature. There is no heat and momentum loss model incorporated into this study, and the detonation initiation process is highly idealized. Hinkey et al.[40] measured a specific impulse of 185 s for stoichiometric H_2/O_2 in a detonation tube at $p_i = 1$ atm and $p_a = 1$ atm ($\psi = 1$) using endwall pressure integration. An optimized Shchelkin spiral was utilized to minimize detonation transition length in that experiment. More recently, the work of Kiyanda et al.[41] has shown that the impulse for stoichiometric H_2/O_2 propellant is largely insensitive to initiation technique. Additionally, Laviolette et al.[42] reported specific impulse measurements, using a pendulum technique, for stoichiometric H_2/O_2 mixtures (again at $\psi = 1$) for a range of L_t/D_t ratios. The mixture was ignited by a weak spark, with transition to detonation occurring within the first tube diameter. The authors obtained specific impulses of 172 s at $L_t/D_t = 19.45$, 153 s at $L_t/D_t = 33.23$, and 133 s at $L_t/D_t = 52.6$. These results are significantly below the corresponding value of 192 s predicted by the idealized CFD model in this study. However, Laviolette et al.,[42] as well as Radulescu et al.[43] in their recent paper, showed the significant effect of heat loss on single-pulse PDE performance, particularly at large L_t/D_t. The latter authors incorporated a simplified heat-loss model into both a simplified, constant-γ method of characteristics code as well as a modified version (using C_2H_4/O_2) of the finite rate chemistry CFD code of the current study. The authors showed how the heat-loss model can significantly improve agreement between predicted and experimentally measured impulse from the literature. Additional details of the changes to the current CFD code, and comparisons with temperature, OH concentration, and velocity measurements, can be found in Refs. 44 and 45.

Additionally, Cooper and Shepherd[11] have recently published the results of an experimental study of single-pulse PDE performance over a wide range of pressure ratios. They utilized a detonation tube filled with stoichiometric C_2H_4/O_2 at 80 kpa initial pressure and an ambient gas of air at pressures ranging from 1.4 to 100 kPa. Impulse was measured via a pendulum technique. Although the propellant and ambient gases of that work differ with those of the current study, it is worthwhile to compare the results in an approximate, relative

fashion at the highest pressure ratios where the effect of the choice of propellant and ambient gas becomes less important. The data reported by Cooper and Shepherd show that, at $\psi = 57$, an $L_e = 0.6L_t$ straight extension improves impulse by ~13% over a baseline detonation tube, whereas a CD nozzle ($\varepsilon = 12$) improves performance by ~35%. In comparison, by examining Table 2 at $\psi = 50$, we can estimate that the model of this study would yield a roughly 8.2% increase in impulse for geometry B (assuming $\upsilon = 1.6$) over geometry A. The model for geometry D, with $\varepsilon = 12$, yields a 34% improvement. Thus, in a limited and relative comparison at high pressure ratios, the model appears to match well with CD nozzle experimental impulse measurements. The agreement in the straight extension case is not as good, though a definitive comparison would necessarily require an exact duplication of the test geometry and conditions.

Equivalent SSRE Model and Performance Comparison

It is instructive to compare the specific impulse of a PDRE fitted with a CD nozzle with an SSRE under equivalent modeling assumptions. Although frozen and equilibrium rocket performance calculations can be readily obtained from the CEA code, these results are not directly comparable to the finite rate chemistry model used in the current PDRE code. The primary concern is the tendency for chemistry to slow down in real nozzle systems as the temperature and pressure are reduced in the expansion process. Thus, it is best to compare the finite rate PDRE systems with a finite rate SSRE model. This SSRE CFD model is heavily derived from the PDRE code. The $L_t = 20$ cm detonation tube is replaced with a thrust chamber 0.1 cm in length and 4.0 cm in diameter (Fig. 13). This thrust chamber then converges at a constant 15-deg angle, over a length of 4.13 cm, to a throat $D^* = 1.787$ cm in diameter. After the throat, the nozzle diverges at 15 deg to a length specified by the user. Thus, the throat diameter and nozzle expansion rate of the SSRE model closely match that of PDRE geometry C. The equilibrium temperature, pressure, and composition of stoichiometric H_2/O_2, burned at constant pressure and enthalpy from $p_i = 1$ atm and $T_i = 300$ K, form a reservoir for a subsonic inflow boundary condition into the domain. Thus, this analysis assumes that the propellant feed system of the SSRE model is the same that for the PDRE.

Similar to the PDRE nozzle optimization study, the finite rate SSRE CFD model is run at various ε until the optimum specific impulse is obtained for a given ψ. However, because the solution converges to steady-state in this model, flowfield information from the highest pressure ratio case can be used to guide area selection at the lower pressure ratios. In each case, the SSRE model is run until the solution converges. In general, the specific impulse and optimum expansion ratio using finite rate chemistry are slightly larger than that for frozen chemistry. Additionally, if the chemistry is frozen in the SSRE CFD model, there is excellent agreement (to within 0.3% in specific impulse) with the frozen-chemistry predictions of CEA.

The mixture-based specific impulse for the baseline detonation tube (PDRE geometry A), PDRE geometry C fitted with an optimized fixed CD nozzle (at each blowdown pressure ratio), and the equivalent optimized SSRE system is plotted for $\psi = 1$–1000 in

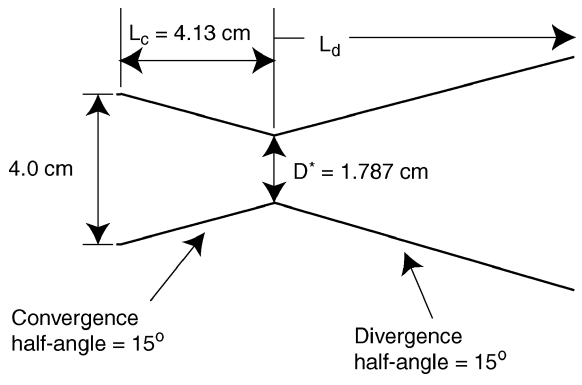

Fig. 13 Schematic of SSRE geometry studied.

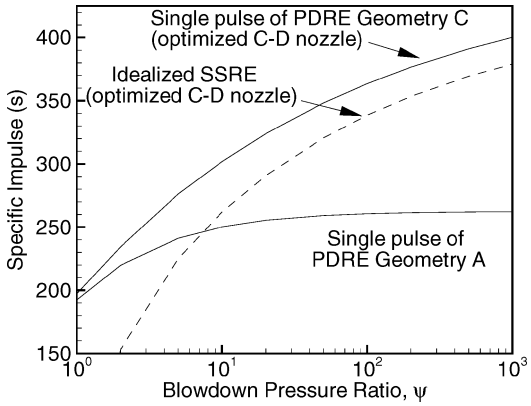

Fig. 14 Finite rate chemistry performance comparison of single-pulse PDREs with an SSRE at the same injection pressure (propellant mixture: stoichiometric H_2/O_2 at $p_i = 1$ atm, $T_i = 300$ K).

Fig. 14. As would be expected from the results discussed earlier, the relative gain from the CD nozzle systems becomes more pronounced at higher pressure ratios. It is noteworthy that a single pulse of both the baseline and CD nozzle PDRE systems outperform an SSRE at $\psi < 7$. This is due to the fact that the relative gain from the extra pressurization provided by the detonation process is greatest in this regime. Thus, the PDRE may have considerable theoretical potential for rocket-type applications when the pressure of the ambient environment is high. Additionally, at higher ψ, a PDRE with an optimized fixed CD nozzle still has a greater specific impulse than an equivalent SSRE. These results indicate that a PDRE equipped with a fixed CD nozzle, though obviously not as efficient at generating thrust as a (theoretical) dynamically adaptive nozzle, can still yield single-pulse performance superior to an equivalent SSRE over a wide range of pressure ratios. Note, however, that this performance gain becomes relatively smaller at higher pressure ratios.

It should be emphasized that these single-pulse comparisons to steady-state engine systems should be considered carefully, because multipulse calculations can yield significantly different results.[8,9] However, in the case of a PDRE system fitted with a CD nozzle, the use of a relatively small nozzle throat (to help limit refill velocity and maintain chamber pressure) may enable multicycle performance near this ideal.[17,46]

Conclusions

A quasi-one-dimensional, finite rate chemistry CFD model for studying PDRE gasdynamics and performance is described and implemented. The single-pulse performance and blowdown time characteristics of four different PDRE geometries are studied over a range of blowdown pressure ratios from 1–1000. The pressure at the endwall is allowed to decay to the ambient value for all simulations in this work. The results show that both straight extensions and CD nozzles can provide valuable improvements to the performance of a baseline detonation tube. However, optimized CD nozzles are generally more effective in increasing performance than straight extensions, particularly at higher pressure ratios. Studies of the blowdown time of the PDRE systems show a strong dependence on pressure ratio for all geometries. Straight extension length will also generally increase blowdown time. Examination of the blowdown history of the optimized CD nozzle geometries shows that the blowdown of these systems could be cut off well before the endwall pressure reaches the ambient value, with an actual slight gain in performance. The single-pulse performance of a PDRE fitted with an optimized fixed CD nozzle is also compared with an SSRE using similar modeling assumptions. The results show that, whereas a PDRE enjoys the largest relative performance gain over an SSRE at low pressure ratios, there is still a noticeable relative advantage for the PDRE at blowdown pressure ratios as high as 1000.

Acknowledgments

This work was supported by the Propulsion Research Center at NASA Marshall Space Flight Center. The author thanks Joe Powers

at Notre Dame for helpful discussions on detonation grid resolution requirements.

References

[1]Eidelman, S., Grossman, W., and Lottati, I., "Review of Propulsion Applications and Numerical Simulations of the Pulsed Detonation Engine Concept," *Journal of Propulsion and Power*, Vol. 7, No. 6, 1991, pp. 857–865.

[2]Kailasanath, K., "Recent Developments in the Research on Pulse Detonation Engines," *AIAA Journal*, Vol. 41, No. 2, 2003, pp. 145–159.

[3]Bratkovich, T. E., Aamio, M. J., Williams, J. T., and Bussing, T. R. A., "An Introduction to Pulse Detonation Rocket Engines," AIAA Paper 97-2742, July 1997.

[4]Sutton, G. P., and Biblarz, O., *Rocket Propulsion Elements*, 7th ed., Wiley, New York, 2001, pp. 27–101.

[5]Kailasanath, K., "A Review of Research on Pulse Detonation Engine Nozzles," AIAA Paper 2001-3932, July 2001.

[6]Cooper, M., Shepherd, J. E., and Schauer, F., "Impulse Correlation for Partially Filled Detonation Tubes," *Journal of Propulsion and Power*, Vol. 20, No. 5, 2004, pp. 947–950.

[7]Li, C., and Kailasanath, K., "Partial Fuel Filling in Pulse Detonation Engines," *Journal of Propulsion and Power*, Vol. 19, No. 5, 2003, pp. 908–916.

[8]Cambier, J.-L., and Tegner, J. K., "Strategies for Pulsed Detonation Engine Performance Optimization," *Journal of Propulsion and Power*, Vol. 14, No. 4, 1998, pp. 489–498.

[9]Yungster, S., "Analysis of Nozzle Effects on Pulse Detonation Engine Performance," AIAA Paper 2003-1316, Jan. 2003.

[10]Guzik, S. M., Harris, P. G., and De Champlain, A., "An Investigation of Pulse Detonation Engine Configurations Using the Method of Characteristics," AIAA Paper 2002-4066, July 2002.

[11]Cooper, M., and Shepherd, J. E., "The Effect of Transient Nozzle Flow on Detonation Tube Impulse," AIAA Paper 2004-3914, July 2004.

[12]Cambier, J.-L., "Preliminary Modeling of Pulse Detonation Rocket Engines," AIAA Paper 99-2659, June 1999.

[13]Mohanraj, R., and Merkle, C. L., "A Numerical Study of Pulse Detonation Engine Performance," AIAA Paper 2000-0315, Jan. 2000.

[14]Mohanraj, R., Merkle, C. L., and Ebrahimi, H. B., "Modeling of Pulse Detonation Engine Operation," AIAA Paper 2001-0475, Jan. 2001.

[15]Wu, Y., Ma, F., and Yang, V., "System Performance and Thermodynamic Cycle Analysis of Airbreathing Pulse Detonation Engines," *Journal of Propulsion and Power*, Vol. 19, No. 4, 2003, pp. 556–567.

[16]Ma, F., Choi, J.-Y., and Yang, V., "Thrust Chamber Dynamics and Propulsive Performance of Single-Tube Pulse Detonation Engines," AIAA Paper 2004-0865, Jan. 2004.

[17]Talley, D. G., and Coy, E. B., "Constant Volume Limit of Pulsed Propulsion for a Constant γ Ideal Gas," *Journal of Propulsion and Power*, Vol. 18, No. 2, 2002, pp. 400–406.

[18]Morris, C. I., "Simplified Analysis of Pulse Detonation Rocket Engine Blowdown Gasdynamics and Performance," AIAA Paper 2002-3715, July 2002.

[19]Ebrahimi, H. B., and Merkle, C. L., "Numerical Simulation of a Pulse Detonation Engine with Hydrogen Fuels," *Journal of Propulsion and Power*, Vol. 18, No. 5, 2002, pp. 1042–1048.

[20]He, X., and Karagozian, A. R., "Numerical Simulation of Pulse Detonation Engine Phenomena," *Journal of Scientific Computing*, Vol. 19, Nos. 1–3, 2003, pp. 201–224.

[21]McBride, B. J., Gordon, S., and Reno, M. A., "Coefficients for Calculating Thermodynamic and Transport Properties of Individual Species," NASA TR TM 4513, 1993.

[22]Petersen, E. L., and Hanson, R. K., "Reduced Kinetic Mechanisms for Ram Accelerator Combustion," *Journal of Propulsion and Power*, Vol. 15, No. 4, 1999, pp. 591–600.

[23]Kee, R. J., Rupley, F. M., and Miller, J. A., "Chemkin-II: A FORTRAN Chemical Kinetics Package for the Analysis of Gas-Phase Chemical Kinetics," Sandia National Laboratories, SAND89-8009, Livermore, CA, Sept. 1989.

[24]Troe, J., "Predictive Possibilites of Unimolecular Rate Theory," *Journal of Physical Chemistry*, Vol. 83, No. 1, 1979, pp. 114–126.

[25]Strang, G., "On the Construction and Comparison of Difference Schemes," *SIAM Journal on Numerical Analysis*, Vol. 5, No. 3, 1968, pp. 506–517.

[26]Oran, E. S., and Boris, J. P., *Numerical Simulation of Reactive Flow*, 2nd ed., Cambridge Univ. Press, Cambridge, UK, 2001, pp. 408–411.

[27]Yee, H. C., "A Class of High-Resolution Explicit and Implicit Shock-Capturing Methods," NASA, TM 101088, 1989.

[28]Grossman, B., and Cinnella, P., "Flux-Split Algorithms for Flows with Non-Equilibrium Chemistry and Vibrational Relaxation," *Journal of Computational Physics*, Vol. 88, No. 1, 1990, pp. 131–168.

[29]Larrouturou, B., "How to Preserve the Mass Fractions Positivity When Computing Compressible Multi-Component Flows," *Journal of Computational Physics*, Vol. 95, No. 1, 1991, pp. 59–84.

[30]Colella, P., Majda, A., and Roytburd, V., "Theoretical and Numerical Structure for Reacting Shock Waves," *SIAM Journal on Scientific and Statistical Computing*, Vol. 7, No. 4, 1986, pp. 1059–1080.

[31]Leveque, R. J., and Yee, H. C., "A Study of Numerical Methods for Hyperbolic Conservation Laws with Stiff Source Terms," *Journal of Computational Physics*, Vol. 86, No. 1, 1990, pp. 187–210.

[32]Poinsot, T. J., and Lele, S. K., "Boundary Conditions for Direct Simulations of Compressible Viscous Flows," *Journal of Computational Physics*, Vol. 101, No. 1, 1992, pp. 104–129.

[33]Gordon, S., and McBride, B. J., "Computer Program for Calculation of Complex Chemical Equilibrium Compositions and Applications," NASA Reference Publ. 1311, 1994.

[34]Shepherd, J. E., "Chemical Kinetics of Hydrogen-Air-Diluent Detonations," Dynamics of Explosions, edited by J. R. Bowen, J.-C. Leyer, and R. I. Soloukhin, Vol. 106, Progress in Astronautics and Aeronautics, AIAA, New York, 1986, pp. 263–293.

[35]Radulescu, M. I., Ng, H. D., Lee, J. H. S., and Varatharajan, B., "The Effect of Argon Dilution on the Stability of Acetylene/Oxygen Detonations," *Proceedings of the Combustion Institute*, Vol. 29, Pt. 2, 2002, pp. 2825–2831.

[36]Yungster, S., and Radhakrishnan, K., "Computational Study of Near-Limit Propagation of Detonation in Hydrogen-Air Mixtures," *Combustion Theory and Modeling*, Vol. 8, No. 4, 2004, pp. 745–770.

[37]Daimon, Y., and Matsuo, A., "Longitudinal Oscillation Mode of One-Dimensional H_2-Air Detonations," AIAA Paper 2004-0794, Jan. 2004.

[38]Powers, J. M., and Paolucci, S., "Accurate Estimates of Fine Scale Reaction Zone Thicknesses in Gas Phase Detonations," AIAA Paper 2005-1171, Jan. 2005.

[39]Wintenberger, E., Austin, J. M., Cooper, M., Jackson, S., and Shepherd, J. E., "Analytical Model for the Impulse of Single-Cycle Pulse Detonation Tube," *Journal of Propulsion and Power*, Vol. 19, No. 1, 2003, pp. 22–38.

[40]Hinkey, J. B., Bussing, T. R. A., and Kaye, L., "Shock Tube Experiments for the Development of a Hydrogen-Fueled Pulse Detonation Engine," AIAA Paper 95-2578, July 1995.

[41]Kiyanda, C. B., Tanguay, V., Higgins, A. J., and Lee, J. H. S., "Effect of Transient Gasdynamic Processes on the Impulse of Pulse Detonation Engines," *Journal of Propulsion and Power*, Vol. 18, No. 5, 2002, pp. 1124–1126.

[42]Laviolette, J.-P., Kiyanda, C. B., and Higgins, A. J., "The Effect of Friction and Heat Transfer on Impulse in a Detonation Tube," Spring Technical Meeting, Canadian Section of the Combustion Inst., Pt. 24, Windsor, ON, Canada, May 2002.

[43]Radulescu, M. I., Morris, C. I., and Hanson, R. K., "The Effect of Heat Loss on the Flow Fields in a Pulse-Detonation Wave Engine," AIAA Paper 2004-1124, Jan. 2004.

[44]Mattison, D. W., Oehlschlaeger, M. A., Morris, C. I., Owens, Z. C., Barbour, E. A., Jeffries, J. B., and Hanson, R. K., "Evaluation of Pulse Detonation Engine Modeling Using Laser-Based Temperature and OH Concentration Measurements," *Journal of Propulsion and Power* (to be published).

[45]Owens, Z. C., Mattison, D. W., Barbour, E. A., Morris, C. I., and Hanson, R. K., "Flowfield Characterization and Simulation Validation of-Multiple Geometry PDEs Using Cesium-Based Velocimetry," *Journal of Propulsion and Power* (to be published).

[46]Kaemming, T. A., and Dyer, R. S., "The Thermodynamic and Fluid Dynamic Function of a Pulsed Detonation Engine Nozzle," AIAA Paper 2004-3916, July 2004.